Spin texture in doped Mott insulators with spin-orbit coupling

Shuai A. Chen ◉,[1] Zheng-Yu Weng ◉,[1] and Jan Zaanen ◉[2]

[1]*Institute for Advanced Study, Tsinghua University, Beijing 100084, China*
[2]*Institute-Lorentz for Theoretical Physics, Leiden University, Leiden P.O. Box 950, The Netherlands*

A hole injected into a Mott insulator will gain an internal structure as recently identified by exact numerics, which is characterized by a nontrivial quantum number whose nature is of central importance in understanding the Mott physics. In this work, we show that a spin texture associated with such an internal degree of freedom can explicitly manifest after the spin degeneracy is lifted by a *weak* Rashba spin-orbit coupling (SOC). It is described by an emergent angular momentum $J_z = \pm \frac{3}{2}$ as shown by both exact diagonalization and variational Monte Carlo calculations, which are in good agreement with each other at a finite size. In particular, as the internal structure such a spin texture is generally present in the hole composite even at high excited energies, such that a corresponding texture in momentum space, extending deep inside the Brillouin zone, can be directly probed by the spin-polarized angle-resolved photoemission spectroscopy (ARPES). This is in contrast to a Landau quasiparticle under the SOC, in which the spin texture induced by SOC will not be protected once the excited energy is larger than the weak SOC coupling strength, away from the Fermi energy. We point out that the spin texture due to the SOC should be monotonically enhanced with reducing spin-spin correlation length in the superconducting-pseudogap phase at finite doping. A brief discussion of a recent experiment of the spin-polarized ARPES will be made.

I. INTRODUCTION

A. Background

A Landau's quasiparticle with a definite momentum, charge, and spin $\frac{1}{2}$ has played a fundamental role in a conventional Fermi liquid. Whether a doped charge (hole) can still propagate like a Bloch wave is important in understanding the two-dimensional (2D) Mott insulator at finite doping. The latter is widely believed to be intrinsically related to the high-T_c superconductor in the cuprate [1,2].

For a single hole injected into a quantum spin antiferromagnetic (AF) background, although earlier studies [2–7] have indicated a Landau-type quasiparticle behavior based on effective approaches, very recently it has been revealed by the unbiased exact diagonalization (ED) and density matrix renormalization group (DMRG) numerical calculations [8–10] that the doped hole will generate a composite structure by twisting the spin background via a nontrivial backflow in the t-J model. Manifestly, a net spin current will further show up due to the presence of a spin-$\frac{1}{2}$ partner around the hole, which gains a nontrivial angular momentum $L_z = \pm 1$ or a new double degeneracy under an open boundary lattice (OBC) with a C_4 rotational symmetry [8].

Such a non-Landau-type novel structure of the composite hole revealed by ED and DMRG calculations can be well reproduced by the variational Monte Carlo (VMC) study [11,12] of a variational ansatz state, which is illustrated in Fig. 1. Generally a net spin $\frac{1}{2}$ will be introduced to the ground state by a doped hole with a characteristic length scale ξ_{sh}. Taking the total $S_z = \frac{1}{2}$ without loss of generality, a net spin current around the hole is generally found as indicated in Fig. 1(a).

Namely, there is an internal relative motion between the doped hole and the surrounding spins, which is characterized by an emergent quantum number, i.e., the angular momentum L_z mentioned above.

The detailed composite structure is further shown in Figs. 1(b) and 1(c) based on the correlators $\langle n_{i_0}^h \bar{S}_i^z \rangle$ and $\langle n_{i_0}^h J_{i,i+\hat{y}}^s \rangle$, which measure the distribution of the net $S_z = \frac{1}{2}$ around the doped hole [Fig. 1(b)] and the corresponding circulating spin current [Fig. 1(c)], respectively. Here $n_{i_0}^h$ denotes the hole number at site i_0, $\bar{S}_i^z$ the summation of two nearest-neighboring spins along the x axis, i.e., $S_i^z + S_{i+\hat{x}}^z$, with i in the opposite sublattice site of i_0 such that a staggered oscillation is smoothened, and $J_{i,i+\hat{y}}^s$ the transverse spin current [cf. Eq. (9)]. The variational ground state [12] [cf. Eq. (7)] is obtained at a lattice of $N = L^2 = 20 \times 20$. The average distance of the $S_z = \frac{1}{2}$ from the hole, ξ_{sh}, is shown in the inset of Fig. 1(b), which is essentially proportional to the spin-spin correlation length ξ of the spin AF background that can be artificially tuned in the VMC calculation (two cases of $\xi \gg L$ and $\xi \sim 2.7$ in units of the lattice constant are shown in the main panel with L denoting the sample length). Then, Fig. 1(c) further shows that the spin current around the hole gets enhanced with reducing $\xi_{sh} \simeq \xi$. It is noted that here we are always focused on the one-hole case in a finite-size sample. If $L \to \infty$, a true AF long-range order $\xi \to \infty$ will set in, such that spin excitations become gapless, which may also contribute to the spin currents induced by the hole in addition to just an $S_z = \frac{1}{2}$ shown in Fig. 1(a) at the finite lattice size. We do not consider this singular limit in the following.

Note that there are two chiralities of the spin currents in the one-hole degenerate ground states corresponding to the novel
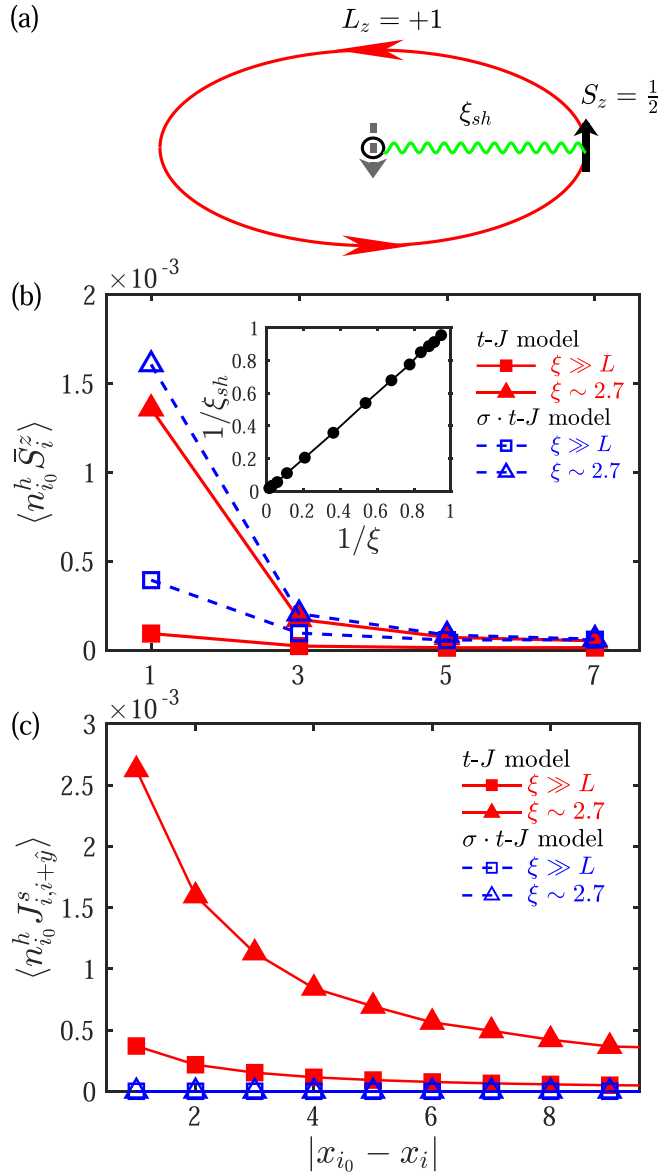
(a)

(b)

(c)

FIG. 1. Composite structure of a doped hole in the pure t-J model of a variational ground-state description [12], which is schematically illustrated by (a) the hole (open circle) is associated with a net spin $S_z = \pm\frac{1}{2}$ of a distance ξ_{sh}, which forms a circulating spin current around the hole. Such a hole composite acquires an angular momentum $L_z = \pm 1$ with novel ground-state degeneracy in agreement with ED and DMRG [8]. (b) Here ξ_{sh} is determined by the hole-spin correlator $\langle n_{i_0}^h \bar{S}_i^z \rangle$ in either the t-J (red solid) or $\sigma \cdot t$-J (blue dashed) model, which shows that $\xi_{sh} \simeq$ spin correlation length ξ (the inset). Note that ξ of the half-filling spin background is tunable, with two limits of long range ($\xi \gg L$) and short range ($\xi \sim 2.7 \ll L$) shown here (cf. Appendix D). (c) The spin current J^s, defined in Eq. (9), around the hole as measured by the correlator $\langle n_{i_0}^h J_{i,i+\hat{y}}^s \rangle$ (along the $\hat{x}$ axis of the lattice) for the t-J (red solid) model, which disappears in the $\sigma \cdot t$-J (blue dashed) model. The VMC calculation is carried out in a finite-size square lattice of $N = L^2 = 20 \times 20$.

quantum number $L_z = \pm 1$ (only $L_z = 1$ is shown here). By contrast, the chiral spin current can be turned off with vanishing angular momentum in the so-called $\sigma \cdot t$-J model, in which the doped hole restores the behavior of a Landau-type
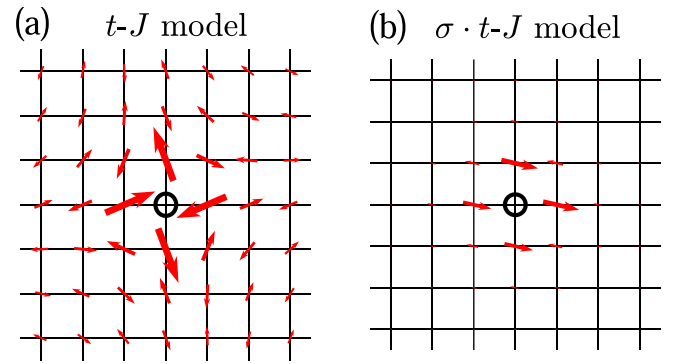
(a) t-J model (b) $\sigma \cdot t$-J model

FIG. 2. A spin-texture pattern induced by a weak SOC, which is frozen into the x-y plane around a doped hole as characterized by a correlator $\langle n_{i_0}^h S_i^{x,y} \rangle$ with i_0 located at the center marked by the open circle. (a) An explicit spin twist in the t-J model; (b) the absence of the spin twist in the $\sigma \cdot t$-J model. Here the half-filling spin background in the variational ground-state study is chosen the same as in Fig. 1 with $\xi \sim 2.7$ and the SOC strength $\lambda = 0.01$ in units of $J = 1$ (see text).

quasiparticle [12]. Here the sole distinction between the t-J and $\sigma \cdot t$-J models is characterized by the nontrivial backflow of spin current in the former, which is absent in the latter with the disappearance of the novelty of the hole composite, although ξ_{sh} remains similar in both cases [cf. Fig. 1(b)].

It is then natural to raise the following question, i.e., how can one detect such an internal quantum structure of the composite hole experimentally? To address this question, in this paper, we introduce a *weak* Rashba spin-orbit coupling (SOC), which may be present in a double-layer system of the cuprate materials like Bi2212 [13]. Then we show that the hidden transverse spin-current pattern appearing around the hole in Fig. 1 can manifest explicitly an emergent semiclassical spin texture lying in the x-y plane, as illustrated in Fig. 2(a). Here a real-space distribution of the correlator $\langle n_{i_0}^h S_i^{x,y} \rangle$ is presented with the hole site i_0 fixed at the center of the sample (denoted by the open circle in Fig. 2). Namely, the unique internal composite structure of the hole in the pure (without SOC) t-J model can be effectively visualized via a frozen transverse spin texture, which is induced by a weak SOC lifting the spin degeneracy and resulting in the locking of S_z with L_z by a total angular momentum $J_z = L_z + S_z$. By contrast, such a transverse spin texture is absent in the $\sigma \cdot t$-J model in the same weak SOC [cf. Fig. 2(b)]. In the latter, the single hole behaves like a Bloch wave without a surrounding spin current (cf. Fig. 1). In the following, we further briefly summarize the main results obtained in this work and their physical implications.

B. Main results

In this work, we show that the hidden spin-current pattern of the spin-$\frac{1}{2}$ partner in a hole composite can manifest itself as an emergent semiclassical spin texture with the introduction of a weak Rashba SOC. It is explicitly exhibited in either the spatial space as indicated by Fig. 2(a) above and the momentum space (see below) as found by ED as well as the VMC calculation.
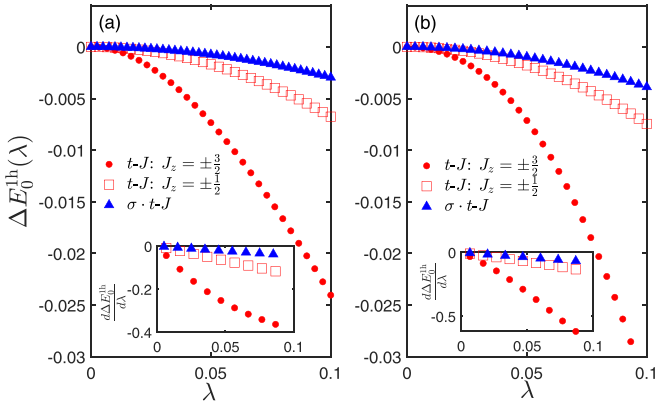
FIG. 3. The energy shift ΔE_0^{1h} due to the SOC for the degenerate ground states ($J_z = \pm\frac{3}{2}$) and first excited states ($J_z = \pm\frac{1}{2}$) obtained by (a) ED and (b) VMC calculations for the t-J (red dot and red square) and $\sigma \cdot t$-J (blue triangle) models. Insets: the first derivation of ΔE_0^{1h} over λ. Here $N = 4 \times 4$ under OBC [cf. Fig. 10(a) for ED under PBC].

As shown in Fig. 2(a), such a spin twist as measured by the correlator $\langle n_{i_0}^h \mathbf{S}_i^{x,y} \rangle$ is formed in the x-y plane around the hole. Physically, it reflects the underlying antiparallel spin alignments in the x-y plane along either the x or y direction across the hole to facilitate the hopping. By a sharp contrast, no such a relative spin twist is shown in Fig. 2(b) for the $\sigma \cdot t$-J model, which is consistent with the absence of a spin-current structure in Fig. 1(c). Note that $\xi \sim 2.7$ is chosen in the VMC calculation such that the distribution of the spin-$\frac{1}{2}$ partner is pulled closer to the hole to enhance the effect in Fig. 2.

The energy shifts of the ground state characterized by $J_z = \pm\frac{3}{2}$ and the first excited one at $J_z = \pm\frac{1}{2}$, together with the ground-state energy shift in the $\sigma \cdot t$-J model, are calculated by both ED and VMC methods as a function of the SOC strength λ, which are in excellent agreement as presented in Fig. 3. Here it is interesting to note that the effect of the SOC in the $\sigma \cdot t$-J model is much weaker than that in the ground-state energy of the t-J model, indicating that the spin-current structure substantially enhances the effect of the Rashba SOC.

Furthermore, under the rotational symmetry, a finite angular momentum J_z in the t-J model also implies a spin-twist structure in momentum space, consistent with the Rashba SOC $\sim \mathbf{S_k} \cdot (\mathbf{k} \times \hat{\mathbf{z}})$ where $\mathbf{S_k}$ denotes a single particle's spin at momentum $\mathbf{k}$. Indeed, in Fig. 4, the spin textures of $\langle \mathbf{S_k} \rangle$ lying in the x-y plane, characterized by a spin helicity in the momentum space, are shown for the ground state of $J_z = \pm\frac{3}{2}$ and the first excited state of $J_z = \pm\frac{1}{2}$, respectively, as calculated by ED. Again, the spin helicity is much weaker for the $\sigma \cdot t$-J model [cf. Fig. 4(a)]. In Fig. 5, the ED and VMC results are further compared in consistency. Both ED and VMC calculations also indicate that the real-space spin texture in Fig. 2(a) can persist into high excited states. At a higher excitation energy, the corresponding spin texture in momentum space will be deeper inside the Brillouin zone, as shown in Fig. 6 obtained by VMC at a larger sample size. Such a holelike quasiparticle with a spin texture in momentum space may be thus directly probed by the spin-polarized angle-resolved photoemission spectroscopy (ARPES) measurement [13].
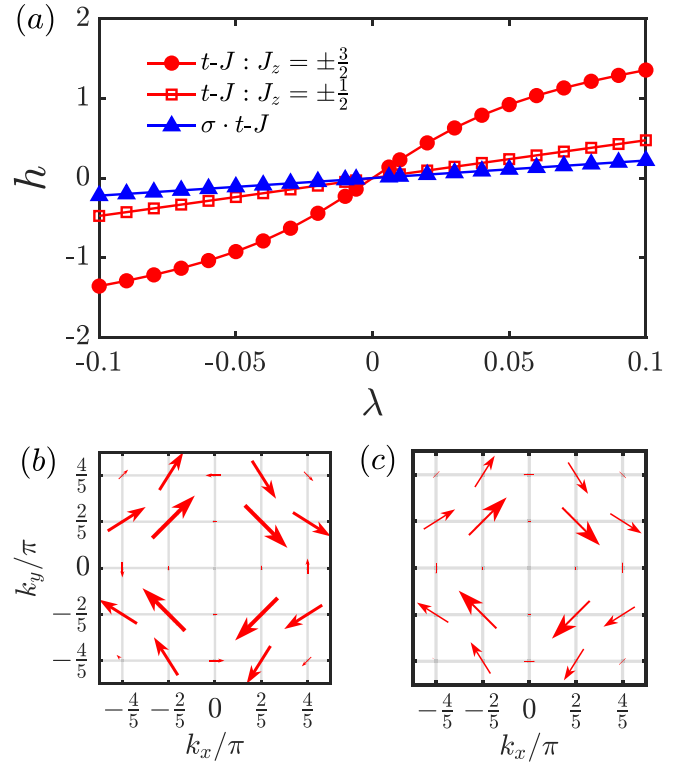

FIG. 4. The spin texture in momentum space. (a) The helicity h defined in Eq. (10) characterizes the overall strength of the spin texture. (b), (c) The corresponding momentum-space spin textures in the ground states ($J_z = \pm\frac{3}{2}$) and the first excited states ($J_z = \pm\frac{1}{2}$) with the same chirality $\chi = +1$ at a positive $\lambda = 0.006$, calculated by ED ($N = 4 \times 4$ under OBC).

The persistence of the spin texture in the Brillouin zone, even close to the Γ point in Fig. 6, is a fact that is in sharp contrast to a Landau Fermi liquid. In the latter, the spin of a quasiparticle may also lock with its momentum to form a spin helicity in the momentum space by SOC. But, it is a single-particle picture without the *spatial* spin texture [cf. Fig. 2(a)], in which the SOC-induced spin helicity is expected to be only robust near the Fermi surface within a very narrow energy interval comparable with the strength of the weak SOC. Away from the Fermi energy, the spin helicity of a Landau quasiparticle can be easily washed away by scattering (cf. Fig. 8) without the protection from the many-body effect in the t-J case as represented by a real-space spin texture associated with $J_z \neq 0$.

Finally, we argue that even though this work has mostly focused on a single hole in a finite-size system, where ED and VMC calculations are available to compare with each other, one may reasonably generalize the main conclusion to the experimentally relevant regime at finite doping. First, it has been shown by the VMC approach that the spin texture amplitude gets enhanced with reducing ξ in the spin background (cf. the inset of Fig. 7), which is due to the fact that the composite of a hole and its spin-$\frac{1}{2}$ partner gets smaller with an enlarged spin current. In order to make quantitative comparison with the experiment [13], aside from the absolute amplitude of the spin-polarized spectral function in the inset, a relative
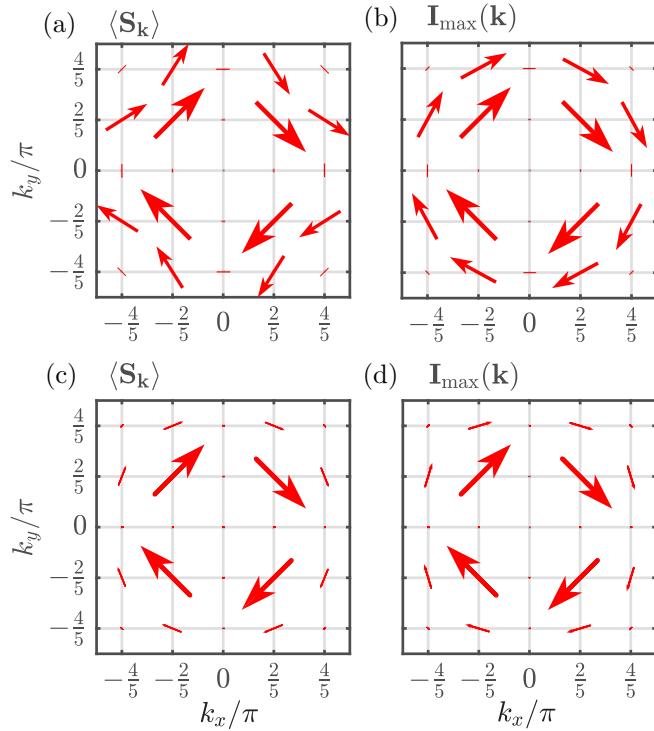
FIG. 5. The spin texture in momentum space. (a), (b) ED results of the spin polarization $\langle \mathbf{S_k} \rangle$ lying in the x-y plane in the ground state and the spin-polarized spectral function $\mathbf{I}_{max}(\mathbf{k})$, respectively. (c), (d) The corresponding VMC results of the variational state ansatz. Here $\lambda = 0.006$ in the t-J-R model on a 4×4 lattice under OBC

FIG. 6. Spin texture in momentum space as manifested in the spin-polarized spectral function $\mathbf{I}_{max}(\mathbf{k})$, which involves the excited states as calculated by VMC in a lattice of 8×8 and $\lambda = 0.01$.

polarization ratio of the spectral function with spin perpendicular to momentum is also shown in the main panel of Fig. 7 at a given momentum, which indeed indicates a comparable strength with the experimental observation [13]. Second, we point out that the pairing of the doped holes with the spin-texture structure obeying the time-reversal symmetry is presumably between the composite holes with the opposite pseudospin $J_z = \pm\frac{3}{2}$ in the presence of SOC. Those other quasiparticle excitations with distinct spin textures, which have higher energies due to the SOC splitting, are thus effectively excluded out of the pair condensate. In such a superconducting-pseudogap regime, predominantly the chiral spin texture associated with the unpaired quasiparticles of $J_z = \pm\frac{3}{2}$ (which exhibit the *same* spin texture in momentum space) will be observed by the spin-polarized ARPES measurement over a finite range of energy, which covers the extended momentum space away from the Fermi surface region. Such a many-body picture clearly illustrates why a quasiparticle excitation with spin texture is "protected," which can survive even when the thermal energy in superconducting-pseudogap regime is dominant over the small energy scale of SOC. By contrast, the emergent Bogoliubov-Landau quasiparticle with Fermi arc [14] should only contribute to a negligible spin texture under a weak SOC.

The rest of paper will be organized as follows. In Sec. II, the t-J and $\sigma \cdot t$-J models with a Rashba SOC are introduced. In Sec. III, we focus on a single hole's motion in a finite-size lattice and discuss the spin-texture structure induced by the SOC based on both ED and VMC approaches. In Sec. IV, a

qualitative discussion at a finite doping is presented. Finally, Sec. V is devoted to the concluding remarks. Various technical details and analyses are presented in Appendices.

II. MODELS

A. The t-J and $\sigma \cdot t$-J models

In this work we shall examine some spin-texture structure hidden in the quasihole excitation of the doped Mott
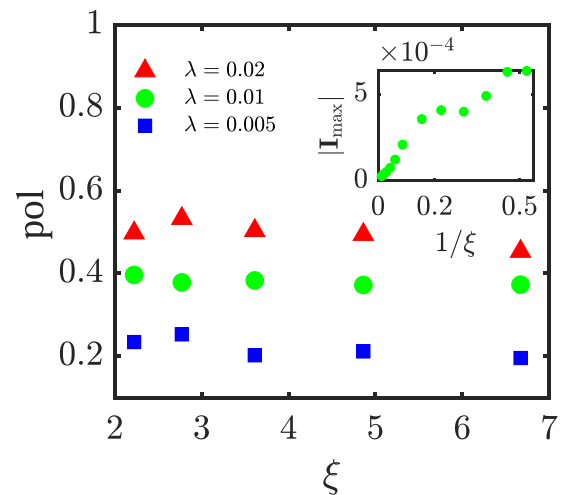
FIG. 7. The relative strength pol$(\omega_c, \mathbf{k})$ of the spectral function with spin polarized perpendicular to the momentum [defined in Eq. (14)] at a given $\mathbf{k} = (\pi/2, \pi/2)$. Here the spin correlation length ξ is taken in a finite range at different λ's (see the text). Inset: The full magnitude of the spectral function $|\mathbf{I}_{max}(\mathbf{k})|$ as a function of ξ. The sample size is 16×16.
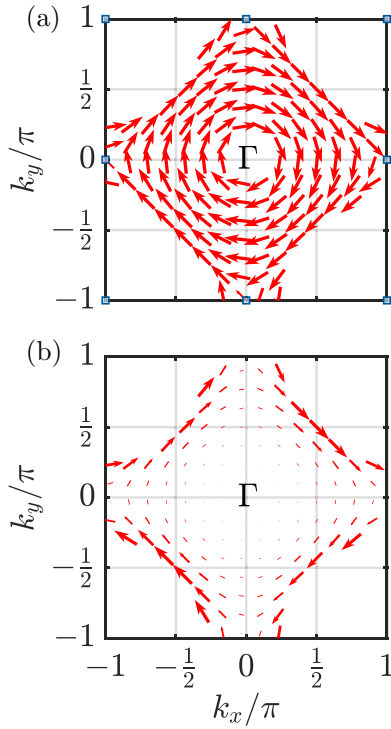
FIG. 8. Spin-texture configuration due to a weak Rashba SOC as determined by the spin-polarized spectral function $\mathbf{I}_{\max}(\mathbf{k})$ for (a) a free Fermi gas, and (b) a Fermi liquid. The spin textures are fragile in the Fermi liquid once the scattering between Laudau's quasiparticle is taken into consideration (cf. Appendix F for the detail).

insulator described by the t-J model [1,15], whose Hamiltonian is composed of the hopping H_t and the superexchange H_J terms as follows:

$$H_t = -t \sum_{\langle ij \rangle, \sigma} c_{i\sigma}^\dagger c_{j\sigma} + \text{H.c.},$$

$$H_J = J \sum_{\langle ij \rangle} \left(\mathbf{S}_i \cdot \mathbf{S}_j - \frac{1}{4} n_i n_j \right), \quad (1)$$

where $\langle ij \rangle$ denotes two nearest-neighbor sites i and j, and $c_{i\sigma}$ creates an electronic hole with the spin index $\sigma = \uparrow$ or $\downarrow$ at site i. $\mathbf{S}_i$ and n_i are the spin and electron number operators, respectively, and the Hilbert space is always subject to the no-double-occupancy constraint

$$n_i \equiv \sum_{\sigma} c_{i\sigma}^\dagger c_{i\sigma} \leqslant 1. \quad (2)$$

At half-filling $n_i = 1$, the system becomes the Mott insulator with the spin degrees of freedom described by the Heisenberg Hamiltonian H_J. We fix the model parameters at $t/J = 3$ and $J = 1$ in the following.

The motion of the holes injected into such a system will strongly interact with the quantum spin background to acquire a Berry-phase-like emergent sign structure, i.e., the so-called *phase string* [16–18]. This singular effect is manifested by generating neutral spin current [8,12] as the backflow associated with the hopping of the doped holes. An important fact is that the spin current is conserved, or the phase string created by the hopping is "irreparable," which replaces the original

fermion signs to become the new statistical signs in the t-J model [18]. One may find a more detailed discussion on the phase-string sign structure in Appendix A.

On the other hand, the phase-string sign structure in the doped t-J model can be precisely eliminated by modifying H_t into the following form [19,20]:

$$H_{\sigma \cdot t} = -t \sum_{\langle ij \rangle, \sigma} \sigma c_{i\sigma}^\dagger c_{j\sigma} + \text{H.c.}, \quad (3)$$

where a spin-dependent sign is inserted to the hopping process, while the superexchange term H_J remains unchanged. It can be shown that the resulting $\sigma \cdot t$-J model with $H_{\sigma \cdot t\text{-}J} \equiv H_{\sigma \cdot t} + H_J$ will no longer generate any spin currents as the phase string is precisely "switched off" (cf. Appendix A). Consequently, an injected hole will behave simply like a Landau quasiparticle with no more internal structure associated with the backflow spin current. Thus, a comparative study of the t-J and $\sigma \cdot t$-J models can provide a unique understanding of the doped Mott physics.

B. Spin-orbit coupling

In this work, we shall introduce a Rashba SOC term as a perturbation, which is given as follows [21]:

$$H_\text{R} = \lambda \sum_i i(c_{i\uparrow}^\dagger c_{i+\hat{y}\downarrow} + c_{i\downarrow}^\dagger c_{i+\hat{y}\uparrow})$$
$$- (c_{i\uparrow}^\dagger c_{i+\hat{x}\downarrow} - c_{i\downarrow}^\dagger c_{i+\hat{x}\uparrow}) + \text{H.c.} \quad (4)$$

Here, the parameter λ characterizes the Rashba SOC strength (valued in units of $J = 1$) and $\hat{x}$ ($\hat{y}$) denotes the unit vector along the x (y) direction. It is noted that a weak Rashba SOC in the cuprate may actually arise from the lack of the inversion symmetry in a double-layer system [13]. In the present approach, we shall neglect the interlayer t-J and SOC coupling between the double layers. Namely, one is still focused on the one-layer problem with only retaining an effective weak intralayer SOC given in Eq. (4), while another layer experiences an opposite SOC [13]. As a perturbation to the t-J or $\sigma \cdot t$-J model, H_R can further provide a locking between the spin and orbital angular momenta in the new Hamiltonian $H_{t\text{-}J\text{-}R} = H_t + H_J + H_R$ or $H_{\sigma \cdot t\text{-}J\text{-}R} = H_{\sigma \cdot t} + H_J + H_R$.

Then, the single-hole problem previously explored by both ED and VMC methods can be easily generalized to the present case, which will reveal interesting properties of the doped hole as a twisted quasiparticle in a rather unique way.

III. SINGLE-HOLE STUDY

As stated in the Introduction, the single-hole ground state of the t-J model has exhibited some highly nontrivial phenomenon as shown by ED and DMRG [8]. Namely, the motion of the hole in the t-J model is always accompanied by a backflow spin current due to the phase-string effect, which then leads to a continuous distribution of momentum for the hole as if there is an incoherent many-body component in addition to a quasiparticle component in a finite-size sample. In the following, we shall examine the response of such a two-component single-hole state to a weak Rashba SOC perturbation by ED and VMC, respectively, which will then

reveal the nature of the internal structure of a doped hole as a unconventional many-body composite in an explicit way.

A. Exact diagonalization and variational ansatz in the absence of SOC ($\lambda = 0$)

To begin with, we note that for one hole injected into a half-filled spin background in 2D, recent ED and DMRG studies in the pure t-J model have clearly demonstrated [8] that the ground state is characterized by an angular momentum $L_z = \pm 1$ and $S^z = \pm \frac{1}{2}$ under OBC. In other words, the single-hole eigenstates are totally fourfold degenerate, which is not only true for the ground state but also valid for the excited states as indicated by ED [8]. It shows that the doped hole acquires an internal structure, which is associated with a chiral spin current. This is in contrast to a Landau's quasiparticle where the many-body effect only leads to a renormalization of its inertia by changing the effective mass without affecting the translational symmetry and U(1) charge nor inducing an internal degree of freedom.

Such a structure associated with the doped hole can be captured by a VMC wave-function ansatz [11,12,22,23]. To understand the unique characterization of this wave-function ansatz, one may first recall a conventional Bloch-wave state given by

$$|\Psi_0\rangle_{1h} = \sum_i \varphi_h^0(i) c_{i\alpha} |\phi_0\rangle, \tag{5}$$

where the single-hole wave function φ_h^0 is a linear combination of the plane wave $\propto e^{\pm i \mathbf{k} \cdot \mathbf{r}_i}$ for a Wannier state $c_{i\alpha} |\phi_0\rangle$. The latter with a single hole at site i is created by annihilating an electron from the translationally invariant half-filling ground state $|\phi_0\rangle$, which may be best approximated by a *bosonic* resonant-valence bond (RVB) state [24] with the spin-spin correlation length $\xi \to \infty$. If the true single-hole ground state with a total momentum $\mathbf{k}$ can be adiabatically connected to Eq. (5) with a finite spectral weight $Z_{\mathbf{k}}$, we may call the hole state a Landau-type quasiparticle.

However, instead of Eq. (5), a single-hole state wave function has been found [12] in good agreement with the above ED and DMRG results [8]. Mathematically, it is realized by replacing the bare hole creation operator c in Eq. (5) with $\tilde{c}$:

$$c_{i\sigma} \to \tilde{c}_{i\sigma} \equiv c_{i\sigma} e^{-i\hat{\Omega}_i}, \tag{6}$$

which leads to a single-hole ansatz state [11,12]

$$|\Psi\rangle_{1h} = \sum_i \varphi_h(i) c_{i\alpha} e^{-i\hat{\Omega}_i} |\phi_0\rangle. \tag{7}$$

Here the nontrivial phase-shift operator takes the form

$$\hat{\Omega}_i = \sum_l \text{Im} \ln(z_i - z_l) n_{l\downarrow}, \tag{8}$$

where $n_{l\downarrow}$ denotes the $\downarrow$-spin operator acting on $|\phi_0\rangle$ with z_l as the complex coordinate of site l. It encodes the mutual braiding between the hole and the $\downarrow$ spins in the background spins, as illustrated in Fig. 1, to give rise to a nontrivial angular momentum $L_z = \pm 1$ and a *net* spin current [12]

$$J_{ij}^s = i(S_i^+ S_j^- - S_i^- S_j^+). \tag{9}$$

The numerical ED and DMRG (up to 8×8) results [8] for the t-J model can be well reproduced by such a variational ground-state ansatz in Eq. (7), with the hole wave function $\varphi_h(i)$ being the variational parameter in the VMC calculation [12]. In Eq. (6), a minus sign is chosen in $\hat{\Omega}_i$, which defines one possible chirality of the ground states. One may also choose a positive sign, i.e., $e^{+i\hat{\Omega}_i}$, to accordingly give rise to a degenerate ground state with the opposite chirality. A detailed symmetry analysis of the wave function in Eq. (7) is given in Appendix B.

By contrast, the Landau-type wave function in Eq. (5) is shown [12] to be a good ground state for the $\sigma \cdot t$-J model, in which the phase-string sign structure is switched off without creating a spin-current backflow during the hopping process [cf. Fig. 1(c)] even though the spin $S_z = \pm \frac{1}{2}$ has a similar distribution around the hole as in the t-J case [cf. Fig. 1(b)]. Obviously, the two wave functions in Eqs. (5) and (7) cannot be adiabatically connected to each other, indicating the qualitative distinction and nonperturbative nature of the single-hole state in comparison with the conventional Landau paradigm. Crucially, the nonlocal phase structure in Eq. (6) persists through the whole spectrum of the single-hole eigenstates irrespective of the excited energy. One may also continuously tune the spin-spin correlation length ξ in $|\phi_0\rangle$ variationally (see Appendix D 1) to simulate the case of an arbitrary finite ξ, which should be self-consistently realized in the ground state at finite doping of holes [22,23]. The detailed structures of the single-hole state as variationally obtained at $\xi \gg L$ and $\xi \sim 2.7$ are illustrated in Figs. 1(b) and 1(c).

After the above brief outline of the single-hole state in the pure case, in the following, one can straightforwardly generalize the above calculations to $\lambda \neq 0$ and study $H_{t\text{-}J\text{-}R}$ by the VMC approach in comparison with the ED results. We will see that the exotic non-Landau-type features of the doped hole will further show up.

B. Single-hole state under a weak Rashba spin-orbit coupling ($\lambda \neq 0$)

1. Exact diagonalization

Let us first start with the ED study under OBC, which is to be compared with a VMC study based on an analytic ground-state ansatz below. In contrast to the ED under the periodic boundary condition (PBC) given in Appendix C 2, the ground-state degeneracy of the t-J model (without SOC) under the OBC (with C_4 symmetry) has been shown to be reduced to fourfold characterized by the orbit angular momentum $L_z = \pm 1$ and spin $S_z = \pm \frac{1}{2}$ [12]. Once λ is switched on in $H_{t\text{-}J\text{-}R}$, S_z and the angular momentum L_z are no longer conserved separately. Instead, the total angular momentum $J_z = L_z + S_z$ will remain as a good quantum number (cf. Appendix C 1), with the ground states characterized by $J_z = L_z + S_z = \pm \frac{3}{2}$ with twofold remaining degeneracy by ED. To show the overall strength of the SOC, the change of the ground-state energy as a function of λ is shown in Fig. 3, in which (a) is for ED and (b) is for VMC (see below). The energy gain induced by SOC as well as the energy splitting between $J_z = \pm \frac{3}{2}$ and $\pm \frac{1}{2}$ is clearly shown here. By contrast, the SOC effect for a quasiparticle in the $\sigma \cdot t$-J model (blue triangles) is much

reduced. A similar result of the ED calculation under PBC can be found in Appendix C 2.

To quantitatively characterize the spin texture induced by $\lambda \neq 0$, one may define a "helicity" as the projection of the averaged spin $\langle \mathbf{S_k} \rangle$ at the direction perpendicular to the momentum $\mathbf{k}$ lying in the x-y plane:

$$h \equiv \sum_{\mathbf{k}} \frac{\langle \mathbf{S_k} \rangle \cdot (\mathbf{k} \times \hat{\mathbf{z}})}{|\mathbf{k}|}, \tag{10}$$

where $\mathbf{S_k} = \frac{1}{2} c_{\mathbf{k}}^{\dagger} \sigma c_{\mathbf{k}}$ with $c_{\mathbf{k}} = [c_{\mathbf{k}\uparrow}, c_{\mathbf{k}\downarrow}]^T$. It measures the strength of locking between the spin and orbit associated with the single hole in the momentum space as shown in Fig. 4(a), with the sign $\chi = \text{sign}(h)$ depicting the chirality of the corresponding spin texture in Figs. 4(b) and 4(c). Here, the helicity h for $J_z = \pm\frac{3}{2}$ (the ground states) shows a significantly larger value as compared to that of the first excited state at $J_z = \pm\frac{1}{2}$ in Figs. 4(b) and 4(c), which both possess the same chirality χ at $\lambda > 0$. The sign of χ does not depend on the sign of J_z but only on the sign of λ as shown in Fig. 4(a). It is easy to understand that the four spin textures in Figs. 4(b) and 4(c) and their counterparts at $\lambda < 0$ just correspond to the eight degenerate eigenstates of the t-J model at $\lambda \to 0$ in the thermodynamic limit or under PBC [8,12], which are split into ground state and the first excitations in a finite lattice under OBC, and further split at $\lambda \neq 0$ with distinct chiralities. On the other hand, the helicity h for the $\sigma \cdot t$-J model is indeed much reduced as shown in Fig. 4(a).

2. Variational Monte Carlo calculation

The above ED calculation shows that by introducing a weak Rashba SOC to lift the separate S_z and L_z degeneracy, the eigenstate degeneracy associated with the hole will be reduced to two with the locking of S_z and L_z in the t-J model. Specifically, the total angular momentum $J_z \equiv L_z + S_z$, which remains to be a good quantum number, will characterize the composite hole $\tilde{c}$ as a *pseudospin* in replacing $S_z = \pm\frac{1}{2}$. Namely, the Rashba SOC will select a new quantum number J_z, which leads to a chiral spin texture. A detailed symmetry analysis is given in Appendix C 1.

In the following, we shall employ a variational wave function to understand the underlying physics involving the many-body response to a weak SOC in the one-hole-doped Mott insulator. By generalizing the previous fourfold degenerate wave functions for the pure t-J model, one may construct the following time-reversal invariant new ground states in terms of the linear combinations of Eq. (7):

$$|\Psi_{\mathrm{R}}\rangle_{\mathrm{1h}} = \sum_i [\varphi_h^{\downarrow}(i) e^{-i\hat{\Omega}_i} c_{i\downarrow} + \varphi_h^{\uparrow}(i) e^{-i\hat{\Omega}_i} c_{i\uparrow}]|\phi_0\rangle, \tag{11}$$

where $\varphi_h^{\uparrow}$ and $\varphi_h^{\downarrow}$ are the variational parameters. One may also construct other types of ansatz by choosing a different factor $e^{\pm\Omega_i}$ in Eq. (11), which variationally produces excited states. The VMC results are presented as follows (see Appendix D 2 for the detail).

A spin texture around the hole has been clearly found to lie in the x-y plane in Fig. 2(a) with $J_z = \pm\frac{3}{2}$ for the t-J model (with $\lambda = 0.01$). Here the spin texture emerges out of the hidden spin-current structure of the non-Landau "twisted"

hole in Fig. 1(a) via SOC. Its scale can be fitted by $\xi_{sh} \simeq \xi$ [cf. the inset of Fig. 1(b)] with ξ_{sh} being the spin-hole correlation length. In Fig. 2, a finite spin-spin correlation length $\xi \sim 2.7$ in $|\phi_0\rangle$ has been used in the VMC. By comparison, one can examine the spin texture in a Landau-type quasiparticle in the $\sigma \cdot t$-J model, i.e., by turning off the phase-string effect in the t-J model. Without creating a spin-current backflow, a doped hole will propagate like a conventional Bloch wave in the $\sigma \cdot t$-J model. At the same strength of $\lambda = 0.01$, there is no more internal spin-texture structure around the hole [see Fig. 2(b)]. Here the variational wave function of the $\sigma \cdot t$-J model is given by

$$|\Psi\rangle_{\sigma \cdot t\text{-}J\text{-}R} = \sum_i [\varphi_h^{\downarrow}(i) c_{i\downarrow} + \varphi_h^{\uparrow}(i) c_{i\uparrow}]|\phi_0\rangle, \tag{12}$$

which is different from those of the t-J model by simply switching off the phase-shift operator $\hat{\Omega}_i$ in Eq. (11).

The overall agreement of the energies between the ED and VMC calculations is further illustrated in Fig. 3, including the energy split between $J_z = \pm\frac{3}{2}$ and $\pm\frac{1}{2}$ in the t-J model and the ground-state energy shift in the $\sigma \cdot t$-J model. One may see the contributions of the SOC to the variational energy shifts in Fig. 3(b) as a function of λ, which are in excellent agreement with the ED results [Fig. 3(a)]. For the $\sigma \cdot t$-J model, in which a Landau's quasiparticle picture can be recovered at $\lambda = 0$ [12], one finds a drastically weakened SOC effect at the same λ as compared to the t-J model. As pointed out above, the latter only differs from the former by the phase-string sign structure as represented by the backflow spin current accompanying the hopping. Similar contrast has been also clearly shown by ED under PBC as presented in Appendix C 2. Therefore, the phase-string effect indeed significantly amplifies the weak Rashba SOC effect in the t-J model.

Furthermore, given the spatial spin texture around the hole in Fig. 2(a), a corresponding spin texture described by the average spin $\langle \mathbf{S_k} \rangle$ in momentum space is expected by the rotational symmetry, which has been already illustrated in, say, Fig. 4(b) at $J_z = \pm\frac{3}{2}$. In Fig. 5, the spin-momentum-locking spin textures obtained by ED and VMC are presented together for comparison, in which $\langle \mathbf{S_k} \rangle$ in the ground state are shown in Figs. 5(a) and 5(c) for a 4×4 lattice.

In Figs. 5(b) and 5(d), we further present the ED and VMC results for the spin-polarized spectral function $\mathbf{I}_{\max}(\mathbf{k})$, which is defined in Eq. (E8) of Appendix E at each given momentum $\mathbf{k}$ with the maximal magnitude of the spectral function via properly adjusting the excited energy. In other words, $\mathbf{I}_{\max}(\mathbf{k})$ can effectively detect the maximal spin texture in momentum space involving the excited states, which is experimentally relevant. In Fig. 6, the spin texture in momentum space is calculated by VMC in a larger (8×8) lattice such that more momentum points are available, where the spin vortex structure is clearly illustrated in the full Brillouin zone, or in other words, persists over the high energy towards the Γ point.

Finally, we emphasize that it is the intrinsic phase string that causes the hole dressed by a surrounding spin current of the $S = \frac{1}{2}$ partner, and the weak Rashba SOC only lifts the degeneracy to induce spin texture by breaking the spin rotational symmetry. If one starts with the large-U Hubbard model, the high-order corrections to the t-J model may be at

the same order as λ, but they do not break the spin rotational symmetry like the SOC does and it has been shown [25] that the phase-string effect is still present. The present conclusion should thus be expected to remain unchanged.

IV. DISCUSSION: FINITE DOPING

For the single-hole case studied in the previous section, the spin-$\frac{1}{2}$ partner forms a spin-current vortex surrounding the hole as illustrated in Fig. 1, which is then "frozen" into a spin texture lying in the x-y plane via a weak SOC as shown in Fig. 2(a). The excellent agreement between the ED and VMC methods clearly indicates that the single-hole ansatz wave function well captures the *intrinsic* structure of the doped hole in a finite-size lattice that cannot be adiabatically connected to a Landau-type quasiparticle, not only in the absence of SOC, but also in the presence of a weak Rashba SOC.

Recently, the VMC approach has been further generalized to the two-hole states in the absence of SOC [26,27]. By forming a tightly bound pair, the chiral spin current gets canceled and the ground state becomes nondegenerate with angular momentum $L_z = 2$ and a d-wave pairing symmetry (cf. Ref. [27]), which is also consistent with the ED and DMRG result [8]. According to the above discussion, in the absence of the chiral spin current, a weak SOC usually should not be able to induce a spin texture in a pairing state of holes in contrast to a single-hole case. Therefore, at finite doping, the spin texture associated with a doped hole is expected to appear only when the unpaired holes are present in an excited state.

Two questions remain to be answered. One concerns the SOC effect in the thermodynamic limit, e.g., in the AF long-range-ordered state with $N = L^2 \to \infty$ and $\xi \to \infty$, where ED certainly does not apply. The VMC calculation indicates that the SOC effect should get diminished continuously as the spin current associated with the spin $\frac{1}{2}$ spreads over in space with the increase of $\xi_{sh} \simeq \xi$. However, in a true AF long-range-ordered state, the gapless spin excitations from the spin background can be further excited to form an even stronger spin current around the hole. In such a limit, the strong spin fluctuations may even cause the self-localization of the doped hole [12], leading to a very singular effect in response to an SOC, which is beyond the present VMC approach at a finite size. On the other hand, the spin texture as the internal structure of the doped hole discussed in this work is expected to be robust if ξ becomes finite in the spin background with $L \gg \xi$. What we have explored here is actually about how a hole moving in a spin background of finite ξ. For example, the ED results of a single hole on a 4×4 lattice may be roughly understood as a finite doping $\sim \frac{1}{16}$ system. As a matter of fact, the variational single-hole state in Eq. (7) may be created in a spin background $|\phi_0\rangle$ whose spin-spin correlation length ξ can be artificially tuned (cf. Appendix D 1). For instance, to better illustrate the spin texture around the hole in Fig. 2(a), a variational $|\phi_0\rangle$ with a finite $\xi \sim 2.7$ has been used. Since $\xi_{sh} \simeq \xi \ll L$ in this case, the spin texture as the integral part of the hole composite is clearly shown in Fig. 2(a). In other words, if a finite doping mainly changes the spin background into a short-range AF state (or spin liquid) with the doped hole still described by $\tilde{c}_{i\sigma}$ in Eq. (6), the above account of

the Rashba SOC effect should be valid in the leading order of approximation.

So the second question will be whether the present study of the single-hole behavior under the Rashba SOC can be meaningfully generalized to the quasiparticle excitation at finite doping, where a short-range AF state with finite ξ will set in. Namely, a single-particle excitation above the ground state $|\Psi_G\rangle$ (which may be either a superconducting or pseudogap state at finite doping, see below) may be constructed by

$$|\psi\rangle_{\text{qp}} = \sum_i \varphi_h(i) \tilde{c}_{i\sigma} |\Psi_G\rangle, \tag{13}$$

similar to the one-hole state in Eq. (7) with replacing the "vacuum" state $|\phi_0\rangle$ by $|\Psi_G\rangle$. We shall delay the discussion of such a second question for a moment. Let us first assume that Eq. (13) is indeed valid, in which $|\Psi_G\rangle$ may be still treated as a short-ranged AF state $|\phi_0\rangle$ with the spin correlation length ξ tunable. Then, one may further make an estimation of the strength of the SOC effect on the quasiparticle excitation as follows.

The spin-polarized spectral function corresponding to the quasiparticle excitation in Eq. (13) will be then approximately treated similar to that of the single-hole case under the SOC (cf. Appendix E). The spin-texture profile, determined by VMC in the momentum space based on $\mathbf{I}_{\text{max}}(\mathbf{k})$, is similar to Fig. 6 with the magnitude depending on ξ and λ. In Fig. 7, a relative strength of the spin texture at $\mathbf{k} = (\pi/2, \pi/2)$ is shown as a function of ξ at various λ's, which is defined by [13]

$$\text{pol}(\omega_c, \mathbf{k}) \equiv \frac{\mathcal{A}_{\sigma_\perp}(\omega_c, \mathbf{k}) - \mathcal{A}_{\bar{\sigma}_\perp}(\omega_c, \mathbf{k})}{\mathcal{A}_{\sigma_\perp}(\omega_c, \mathbf{k}) + \mathcal{A}_{\bar{\sigma}_\perp}(\omega_c, \mathbf{k})}, \tag{14}$$

in terms of the spin-polarized ARPES spectral function $\mathcal{A}_\sigma(\omega, \mathbf{k})$ at energy ω with spin index σ [defined in Eq. (E1) in Appendix E]. Note that here $\sigma_\perp$ denotes the spin polarization perpendicular to $\mathbf{k}$ ($\bar{\sigma}_\perp = -\sigma_\perp$) and ω_c the frequency at which the intensity reaches its maximum. As Fig. 7 shows, $\text{pol}(\omega_c, \mathbf{k})$ is roughly flat in a range of finite ξ with the strength monotonically dependent on λ, which is comparable to the experimental measurement in the cuprate [13]. Note that pol here only measures the relative spin polarization perpendicular to $\mathbf{k}$. In the inset of Fig. 7, the total strength of the spectral function $|\mathbf{I}_{\text{max}}|$ (cf. Appendix E) at the same $\mathbf{k} = (\pi/2, \pi/2)$ is also shown as a function of ξ as $\xi \to \infty$, which eventually approaches zero at the AF long-ranged-order limit. Physically, it may be understood as the spin current carried by the spin-$\frac{1}{2}$ partner of the hole composite becomes less and less concentrated around the hole to result in the reducing SOC effect at large ξ and L.

Now let us come back to address the above second question about the single-particle excitation at finite doping. We point out that the single-hole ground-state ansatz [Eq. (7)] can be actually regarded as the few hole special cases [11,12,26,27] of a general ground-state ansatz previously proposed to describe the SC and pseudogap phase at finite doping [22,23]:

$$|\Psi_G\rangle = \hat{\mathcal{D}}^{\frac{N^h}{2}} |\text{RVB}\rangle, \tag{15}$$

in which the AF vacuum state $|\phi_0\rangle$ is self-consistently re-placed by $|RVB\rangle$, which is AF short-range ordered at a finite doping. Here the N^h holes are paired up and created by

$$\hat{\mathcal{D}} = \sum_{ij} g_{ij} \tilde{c}_{i\uparrow} \tilde{c}_{j\downarrow}, \qquad (16)$$

where $\tilde{c}$ defined by Eq. (6) describes the doped holes as twisted (non-Landau) quasiparticles. Here $|\Psi_G\rangle$ is intrinsi-cally superconducting at $T = 0$ in a finite concentration of holes. The excitations of free unpaired spinons in $|RVB\rangle$ can eventually destroy the SC phase coherence, resulting in the so-called lower pseudogap phase (LPP) or spontaneous vortex phase, where the pairing in terms of the twisted quasiparticles, i.e., $\langle\hat{\mathcal{D}}\rangle \neq 0$, is still present, but the true Cooper pairing order parameter vanishes [22,23].

Naturally, an elementary quasiparticle excitation can be constructed, based on $|\Psi_G\rangle$, as composed of the unpaired twisted quasiparticle given in Eq. (13). In particular, since the twisted quasiparticles are paired up via $\hat{\mathcal{D}}$ in $|\Psi_G\rangle$, the latter may be reasonably considered to be a "vacuum" as far as $\tilde{c}$ is concerned in Eq. (13), which thus resembles a $|\phi_0\rangle$ just like the single-hole state in Eq. (7) except for a finite ξ. Furthermore, turning on the Rashba SOC in $H_{t\text{-}J\text{-}R}$ with $\lambda \neq 0$, there will be an additional important effect occurring in the SC/LPP at finite doping, which can further enhance the spin-texture structure found in the single-hole case, besides the reducing ξ discussed above, as to be outlined below.

Note that in the above SC/LPP ansatz states, the pair-ing between the twisted quasiholes of $\tilde{c}_{i\sigma}$ with $\sigma = \uparrow, \downarrow$ will be modified by the SOC with the degenerate ground states characterized by a time-reversal pair of new good quantum numbers: $J_z = \frac{3}{2}$ and $-\frac{3}{2}$, i.e.,

$$\hat{\mathcal{D}} \rightarrow \sum_{ij} g(i, j) \tilde{c}_{i, J_z=3/2} \tilde{c}_{j, J_z=-3/2}. \qquad (17)$$

As we have seen, the twisted hole states with both $J_z = \pm\frac{3}{2}$ have the same chirality of the spin texture. In Eq. (17), the low-lying excitations will be mainly dominated by those un-paired quasiparticles of $J_z = \pm\frac{3}{2}$ with the same spin texture, where the other excited states with opposite chirality in the single-hole problem should no longer be stable to contribute to the spin polarized $\mathbf{I}_{max}$ shown in Fig. 6. Thus, $\mathbf{I}_{max}$ is expected to be further enhanced due to the fact that the twisted quasiparticles of $J_z = \pm\frac{3}{2}$ are uniquely singled out via the pairing condensation in $|\Psi_G\rangle$ to exclude all those excitations of opposite spin textures split by the SOC.

V. CONCLUDING REMARKS

As the precursor of a non-Fermi liquid, it has been found recently [12,27] that a hole injected into a quantum AF spin background will behave like a non-Landau quasiparticle. It is a hole composite in which the neighboring spin background will get "twisted" by the phase-string sign structure to facil-itate the hopping of the hole. In the single-hole ansatz state (7), such a many-body effect is well captured by the nonlocal phase-shift factor $e^{-i\hat{\Omega}_i}$. In particular, such a structure can become explicitly manifested if an extra $S_z = \pm\frac{1}{2}$ (introduced by the hole doped into the spin-singlet background) is nearby

in a finite system, which will form a spin current swirling around the hole like in an atom with a nontrivial angular momentum $L_z = \pm 1$.

Then, we have shown in this work that by introducing a weak Rashba SOC to lift the spin-$\frac{1}{2}$ degeneracy associated with the doped hole, the spin current will be turned into a semiclassical chiral spin texture lying in the x-y plane in both real and momentum space, which is characterized by a new quantum number $J_z = L_z + S_z$. It is important to emphasize that a weak SOC does not change the essential internal struc-ture of the hole composite, but mainly affects the "soft" spin current contributed by the degenerate $S_z = \pm\frac{1}{2}$, which are locked with L_z due to breaking the spin rotational symmetry by SOC. In this sense, the present VMC approach is perturba-tivelike based on the *good* (variational) solutions in the pure t-J and $\sigma \cdot t$-J models. In particular, the semiclassical spin texture formed by the spin $\frac{1}{2}$ around the hole in Fig. 2(a) is merely a "fingerprint" that explicitly reveals the underlying quantum many-body hole-spin entanglement, which already exists in the absence of SOC. A recent proposal of the so-called rotational ARPES spectra [28] may be also used to probe such an internal spin structure associated with the doped hole.

By using ED and VMC methods, such a spin-texture pat-tern characterized by the new quantum number J_z has been confirmed by both exact numerics and the variational wave function. The excellent agreement between the ED and VMC results shows that the hole composite for the t-J model has properly captured the essence of a doped Mott insulator in response to a perturbation of the SOC. On the other hand, by precisely turning off the phase string in the $\sigma \cdot t$-J model, both ED and VMC calculations also demonstrate the disappear-ance of the novelty of the non-Landau quasiparticle, with a substan-tially weakened spin texture entirely induced by the Rashba SOC for a Landau-type quasiparticle.

Furthermore, we have argued that such a chiral spin texture in the t-J model may become directly observable at finite doping in the superconducting-pseudogap regime, where the majority of the doped holes form a paired condensate, which effectively selects the hole composites with opposite quan-tum numbers $J_z = \pm\frac{3}{2}$ in a weak Rashba interaction with the same chiral spin texture. In particular, by making the spin AF background short ranged, the hole composite becomes "atomlike" as a truly bound entity such that the spin texture around the hole is both amplified by the Rashba effect and independent of the lattice size. Consequently, the low-lying quasiparticles excited from the paired condensate will be pre-dominately characterized by the same spin-texture structure in momentum space, which may be well observed by the spin-polarized ARPES in momentum space, extending deep inside the Brillouin zone away from the Fermi energy. Of course, we caution that the present discussion of the finite doping phase is mostly based on a generalization of the single-hole problem. A further microscopic study at the same level as dealing with the emergent Bogoliubov-Landau quasiparticle with Fermi arc [14] will be desirable to describe the spin-texture structure under a weak SOC.

It is important to note that even though a similar spin texture in momentum space (but not in the real space) com-mensurate with the Rashba SOC can be simply found in a

noninteracting band structure model as shown in Fig. 8(a) (cf. Appendix F), the spin texture is actually well protected only within a very narrow energy regime near the Fermi surface decided by the SOC strength λ. As illustrated in Fig. 8(b), the spin texture at momenta away from the Fermi surface becomes much fragile in a Fermi-liquid theory due to a general scattering effect on the quasiparticles once the excitation energy is higher than a small scale set by the SOC splitting energy (cf. Appendix F).

We comment on a recent experimental result of the spin-polarized ARPES experiment on the high-T_c cuprate of the Bi-2212 compound [13] in the pseudogap regime with a $J \sim 120$ meV. The dependence of the in-plane spin polarization on the quasiparticle momentum observed in the experiment seems to be compatible with a weak Rashba SOC strength as studied in this work, which presumably comes from the double-interlayer structure [13]. It is an important observation that the spin polarization extends deep towards the Γ point of the Brillouin zone, which is hard to understand from a conventional Fermi-liquid theory. As discussed above, the spin texture found in the spin-polarization measurement should be restricted by a characteristic energy scale due to the SOC of a single quasiparticle, which is rather small (e.g., $\lambda \sim 0.01J \sim 1.2$ meV) and determines a very narrow regime in the momentum space near the Fermi energy. By contrast, the spin texture of the new quasiparticle in a doped Mott insulator is more intrinsically associated with the internal structure of the doped hole, which is present even for the high-energy excitations. An entirely different mechanism due to quantum many-body correlations is at work here.

Finally, along with the SOC that breaks the spin rotation, we point out another important effect involving the Zeeman field, which also breaks the spin rotational symmetry. Such a Zeeman effect acts on the whole neutral spin background, in contrast to SOC mainly coupling a hole with its surrounding spins. Although no spin texture is expected, the Zeeman effect that polarizes spins can exert strong influence on the charge degree of freedom via an enhanced spin current due to the enlarged net spin S_z. Such an important effect due to phase string is currently under study elsewhere.

ACKNOWLEDGMENTS

APPENDIX A: SIGN STRUCTURES IN THE t-J AND $\sigma \cdot t$-J MODELS

To be self-contained, in the following we briefly outline the phase-string sign structure in the t-J model and the absence of it in the $\sigma \cdot t$-J model [16–18].

In the t-J model, the Fermi sign structure vanishes at half-filling due to the no-double-occupancy constraint or the "Mottness." Upon doping, a reduced Fermi sign structure starts to recover with the increase of doping concentration of holes. Specifically, the partition function for the t-J model on

a square lattice at an arbitrary doping can be expressed by

$$Z_{t\text{-}J} = \sum_c \tau_c \mathcal{Z}[c], \tag{A1}$$

where the summation is over c, denoting the set of closed loops of the spatial trajectories of all spins and holes. Accompanying a non-negative weight $\mathcal{Z}[c] \geqslant 0$, each path c is associated with a sign factor τ_c given by

$$\tau_c \equiv (-1)^{N_h^{\downarrow}[c]} \times (-1)^{N_h^h[c]}. \tag{A2}$$

Here the Berry's phaselike τ_c replaces the usual fermion signs in a partition function of a fermion system due to an explicit restriction of the Mottness. In τ_c, $(-1)^{N_h^h[c]}$ resembles a conventional Fermi sign structure now only associated with the doped holes, while $(-1)^{N_h^{\downarrow}[c]}$ depends on the total parity of exchanges between the holes and $\downarrow$ spins for the closed path set c, which is known as the phase-string sign structure.

By contrast, in the $\sigma \cdot t$-J model, the phase-string sign structure can be simply *switched off* such that the partition function is reduced to

$$Z_{\sigma \cdot t\text{-}J} = \sum_c (-1)^{N_h^h[c]} \mathcal{Z}[c], \tag{A3}$$

where the non-negative weight $\mathcal{Z}[c]$ remains the *same* as in the t-J model, with the same Fermi sign structure of the holes: $(-1)^{N_h^h[c]}$. At half-filling, the t-J and $\sigma \cdot t$-J models both reduce to the Heisenberg model.

Therefore, the distinction between the t-J and $\sigma \cdot t$-J models only emerges upon doping, which is solely distinguished by the phase-string sign structure $(-1)^{N_h^{\downarrow}[c]}$ in Eq. (A2). As it turns out, such a phase string is very singular, which prevents a perturbative treatment of the t-J model, even in the one-hole-doped case. In the next Appendix, we shall discuss a duality transformation and an emergent symmetry in the one-hole ground state, which are entirely due to the phase-string effect in a nonperturbative way.

APPENDIX B: ONE-HOLE WAVE-FUNCTION ANSATZ AND EMERGENT SYMMETRY IN THE t-J MODEL

The Mott physics in the pure t-J model is crucially associated with an emergent phase-string sign structure as outlined above, which will result in a nonperturbative duality transformation and a new type of ground-state ansatz [11,12]. In the following, we concentrate on such a one-hole problem from the perspective of symmetry.

To account for the phase-string effect in the one-hole case, a many-body phase-shift factor $e^{\pm i\hat{\Omega}_i}$ produced by the doped hole has to be introduced [11,12] in Eq. (6), with $\hat{\Omega}_i$ defined in Eq. (8). The fourfold-degenerate one-hole ground states can be constructed with $|\Psi_G\rangle_{1,2}$ by removing a $\downarrow$ spin and $|\Psi_G\rangle_{3,4}$ by removing an $\uparrow$ spin from the half-filling ground state $|\phi_0\rangle$ as follows:

$$|\Psi\rangle_{1,2} = \sum_i \varphi_{1,2}(i) e^{\mp i\hat{\Omega}_i} c_{i\downarrow} |\phi_0\rangle, \tag{B1}$$

$$|\Psi\rangle_{3,4} = \sum_i \varphi_{3,4}(i) e^{\mp i\hat{\Omega}_i} c_{i\uparrow} |\phi_0\rangle. \tag{B2}$$

Here the variational parameters $\varphi_{1,2,3,4}(i)$ only depend on the hole's position. The variational ansatzes in Eqs. (B1) and (B2) divide the single-hole Hilbert space into four sectors. The VMC simulation and analytic analysis have shown [12], consistent with the ED and DMRG results, that aside from $S_z = \frac{1}{2}$ for $|\Psi_G\rangle_{1,2}$ and $S_z = -\frac{1}{2}$ for $|\Psi_G\rangle_{3,4}$, each of them acquires additional double degeneracies with nontrivial orbital momenta $L_z = \pm 1$, respectively, for a bipartite lattice of $N = 2M \times 2M$.

The phase-shift factors $e^{\mp i\hat{\Omega}_i}$ in Eqs. (B1) and (B2) characterize the mutual entanglement between the hole and spins in the AF background $|\phi_0\rangle$ to precisely keep track of the phase-string structure. Explicitly, we can make a choice $\hat{\Omega}_i = \sum_l \mathrm{Im}\ln(z_i - z_l)n_l^{\downarrow}$, as in Eq. (8) for a 2D system. It represents a mutual duality transformation, which cannot be perturbatively obtained based on a bare hole state created by $c_{i\sigma}$ on $|\phi_0\rangle$. With the nontrivial many-body effect encoded in $e^{\mp i\hat{\Omega}_i}$, the resulting $\varphi_{1,2,3,4}(i)$ are consequently treated as the single-hole wave functions in the VMC calculation, which have turned out to be a very good approximation [12].

Given the single-particle nature, nevertheless, $\varphi_{1,2,3,4}(i)$ are not simply Bloch wave functions. By a symmetry analysis, we show some intrinsic topological relations among them in the following.

The antiunitary time-reversal symmetry $\mathcal{T}$ flips spin direction by

$$\mathcal{T}c_{\uparrow}\mathcal{T}^{-1} = c_{\downarrow}, \quad \mathcal{T}c_{\downarrow}\mathcal{T}^{-1} = -c_{\uparrow}, \quad \mathcal{T}i\mathcal{T}^{-1} = -i. \quad \text{(B3)}$$

Then, by noting the time-reversal symmetry in the ground states, one has

$$\mathcal{T}|\Psi_G\rangle_1 = |\Psi_G\rangle_3, \quad \text{(B4)}$$

which requires

$$\varphi_3(i) = -\varphi_1^*(i)e^{i\sum_{l\neq i}\mathrm{Im}\ln(z_i - z_l)}, \quad \text{(B5)}$$

with the opposite $S_z = \pm\frac{1}{2}$ and $L_z = \pm 1$. Similarly, $\mathcal{T}$ transforms the state $|\Psi_G\rangle_2$ into $|\Psi_G\rangle_4$, which results in

$$\varphi_4(i) = -\varphi_2^*(i)e^{i\sum_{l\neq i}\mathrm{Im}\ln(z_i - z_l)}. \quad \text{(B6)}$$

Furthermore, one may also define a unitary symmetry $\mathbb{Z}_2$ generated by the spin-flip operation $\mathcal{R}$, which is defined

$$\mathcal{R}c_{\uparrow}\mathcal{R}^{-1} = c_{\downarrow}, \quad \mathcal{R}c_{\downarrow}\mathcal{R}^{-1} = -c_{\uparrow}, \quad \text{(B7)}$$

with no extra sign change in the imaginary unit i. Then,

$$\mathcal{R}|\Psi_G\rangle_1 = |\Psi_G\rangle_4 \quad \text{(B8)}$$

leads to

$$\varphi_4(i) = -e^{-i\sum_{l\neq i}\mathrm{Im}\ln(z_i - z_l)}\varphi_1(i), \quad \text{(B9)}$$

where $|\Psi_G\rangle_1$ and $|\Psi_G\rangle_4$ have the same $L_z = -1$ and opposite $S_z = \pm\frac{1}{2}$. Similarly, $\mathcal{R}$ transforms the state $|\Psi_G\rangle_2$ into $|\Psi_G\rangle_3$. Table I lists the corresponding quantum numbers of the degenerate ground states $|\Psi_G\rangle_{1,2,3,4}$ and the actions of time-reversal $\mathcal{T}$ and spin-flip symmetries $\mathcal{R}$.

TABLE I. List of the quantum numbers of four degenerate ground states $|\Psi_G\rangle_{1,2,3,4}$ in the pure single-hole doped t-J.

	Phase-string factor	S_z	L_z	J_z	Relation with $|\Psi\rangle_1$
$|\Psi_G\rangle_1$	$e^{-i\hat{\Omega}_i}$	$+\frac{1}{2}$	$+1$	$+\frac{3}{2}$	
$|\Psi_G\rangle_2$	$e^{+i\hat{\Omega}_i}$	$+\frac{1}{2}$	-1	$-\frac{1}{2}$	$\mathcal{RT}|\Psi\rangle_1$
$|\Psi_G\rangle_3$	$e^{-i\hat{\Omega}_i}$	$-\frac{1}{2}$	-1	$-\frac{3}{2}$	$\mathcal{T}|\Psi\rangle_1$
$|\Psi_G\rangle_4$	$e^{+i\hat{\Omega}_i}$	$-\frac{1}{2}$	$+1$	$+\frac{1}{2}$	$\mathcal{R}|\Psi\rangle_1$

APPENDIX C: RASHBA INTERACTION

1. Total angular momentum J_z

The presence of the Rashba interaction breaks conservation of the angular momentum L_z and total spin S_z. However, the total angular momentum $J_z = L_z + S_z$ remains as a good quantum number. Here we give a proof. We aim to prove $UH_{t\text{-}J\text{-}R}U^{\dagger} = H_{t\text{-}J\text{-}R}$ for t-J-R Hamiltonian with $U = \exp(-i\frac{\pi}{2}J_z)$ generated by J_z. For Rashba SOC term $c_{i\uparrow}^{\dagger}c_{i+\hat{x}\downarrow}$ in Eq. (4),

$$
\begin{aligned}
Uc_{i\uparrow}^{\dagger}c_{i+\hat{x}\downarrow}U^{\dagger} &= e^{-i\frac{\pi}{2}(L_z+S_z)}c_{i\uparrow}^{\dagger}c_{i+\hat{x}\downarrow}e^{i\frac{\pi}{2}(L_z+S_z)} \\
&= e^{-i\frac{\pi}{2}S_z}c_{\hat{R}(i)\uparrow}^{\dagger}c_{\hat{R}(i+\hat{x})\downarrow}e^{+i\frac{\pi}{2}S_z} \\
&= -ic_{\hat{R}(i)\uparrow}^{\dagger}c_{\hat{R}(i)+\hat{y}\downarrow},
\end{aligned} \quad \text{(C1)}
$$

where $\hat{R}(i)$ is the site by rotating site i counterclockwisely 90°. Similarly, for term $c_{i\uparrow}^{\dagger}c_{i+\hat{y}\downarrow}$, we have

$$Uc_{i\uparrow}^{\dagger}c_{i+\hat{y}\downarrow}U^{\dagger} = -ic_{\hat{R}(i)\uparrow}^{\dagger}c_{\hat{R}(i)-\hat{x}\downarrow}. \quad \text{(C2)}$$

Combination of Eqs. (C1) and (C2) demonstrates the invariance of Rashba interaction under U,

$$UH_RU^{\dagger} = H_R. \quad \text{(C3)}$$

The hopping and superexchange terms obviously conserve the total momentum J_z. Therefore, we prove that total momentum J_z is a good quantum number for the t-J-R model.

2. ED under periodic boundary condition

We present the ED result under the periodic boundary condition (PBC) in the following. Generally, without SOC, there are eightfold-degenerate ground states distinguished by momenta $\mathbf{k}_0 = (\pm\pi/2, \pm\pi/2)$ with total $S^z = \pm\frac{1}{2}$ in the pure one-hole state [8]. The Rashba SOC will lift the spin degeneracy such that the spin $S = \frac{1}{2}$ will be locked with the four momenta $\mathbf{k}_0$ to give rise to a spin texture of $\langle\mathbf{S_k}\rangle$ lying in the x-y plane as illustrated in Fig. 9(a), which is obtained by ED with a very small SOC strength $\lambda = 0.006J$ (see below). Here, corresponding to a ground state with a given total momentum, say, $\mathbf{k}_0 = (\pi/2, \pi/2)$, $\langle\mathbf{S_k}\rangle$ is mainly concentrated at $\mathbf{k}_0$ as indicated by the solid arrow in Fig. 9(a) similar to a *free* quasiparticle.

However, different from the free quasiparticle picture, in the present ground state, a nontrivial "spin-current" pattern is also found in the momentum space as shown in Fig. 9(b), which is defined by the correlator

$$\langle J_{\mathbf{k},\mathbf{k}'}^s\rangle \equiv i\langle S_{\mathbf{k}}^+S_{\mathbf{k}'}^- - S_{\mathbf{k}'}^+S_{\mathbf{k}}^-\rangle. \quad \text{(C4)}$$
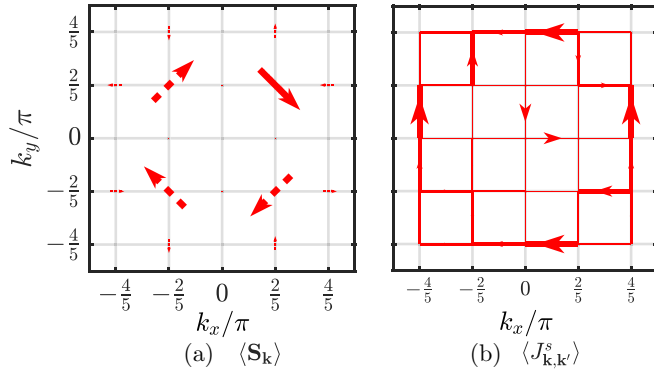
FIG. 9. Two-component structure of the one-hole ground states of the t-J model with a weak SOC ($\lambda = 0.006J$) obtained by ED under PBC in a 4×4 lattice. (a) The total spin $S = \frac{1}{2}$ is locked with four total momenta at $\mathbf{k}_0 = (\pm\pi/2, \pm\pi/2)$. (b) Corresponding to one of the $\mathbf{k}_0$'s in (a) (the full arrow), a "spin current" pattern of $\langle J^s_{\mathbf{k},\mathbf{k}'} \rangle$ in Eq. (C4) indicates a hidden many-body effect (see text).

Here, $\langle J^s_{\mathbf{k},\mathbf{k}'} \rangle$ illustrates correlations between spins at the neighboring momenta (with $\mathbf{k} \neq \mathbf{k}'$), which is present even in the absence of the SOC. The nontrivial spin-current pattern in Fig. 9(b) only disappears in the half-filling due to fully frozen charge degree of freedom and the absence of phase-string effect. Hence, $\langle J^s_{\mathbf{k},\mathbf{k}'} \rangle \neq 0$ represents an incoherent component of the one-hole ground state, which manifests as a broaden momentum distribution of the single hole as a partial momentum can be carried away by the backflow spin current such that the single-particle momentum $\mathbf{k}$ is no longer conserved [8]. This represents the so-called incoherent component violating the Landau's one-to-one correspondence between the momentum $\mathbf{k}$ of the hole and the total momentum $\mathbf{k}_0$. The latter should be always conserved under PBC due to the translational invariance of the total system including all spins and the hole. However, due to the spin current, a partial momentum can be continuously transferred to the spin background from the hole or *vice versa* to result in a non-Landau quasiparticle state, which is essentially a many-body effect [8].

Next, we examine the quantitative role of SOC. Figure 10(a) shows the *change* of the ground-state energy $\Delta E_0^{1h}(\lambda) \equiv E_0^{1h}(\lambda) - E_0^{1h}(0)$ as a function of λ. For the t-J model, the linear-λ dependence (red line) and a *finite* value of its first derivative over λ at $\lambda \to 0$ [cf. the inset of Fig. 10(a)] strongly suggest that the spin texture in Fig. 9 at a very small $\lambda = 0.006J$ is *not* completely new as induced by the SOC, but should rather exist already in the pure t-J model to give rise to the first-order perturbative contribution. Namely, a weak λ here mainly selects and picks up a particular linear recombination state from the pure one-hole ($2 \times 4 = 8$ fold) degenerate ground states in forming the spin texture in Figs. 9(a) and 9(b).

Indeed, by turning off the phase-string effect or the spin-current structure in the t-J model to result in a Landau-type quasiparticle in the $\sigma \cdot t$-J model, the change in ground-state energy due to SOC becomes significantly weakened as comparatively shown by Fig. 10(a) and the inset (blue triangles). There is no more linear-λ term. As a matter of fact, to make the spin-texture amplitude comparable, the SOC strength λ has to be enhanced by two orders of magnitude in $\sigma \cdot t$-J
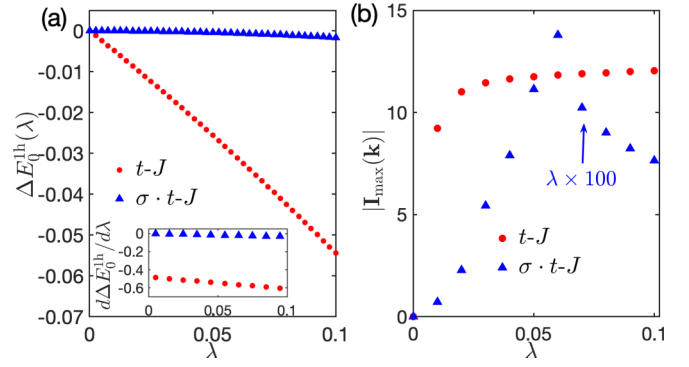

FIG. 10. (a) Ground-state energy shift ΔE_0^{1h} vs the SOC strength λ for the t-J (red dot) and the $\sigma \cdot t$-J (blue triangle) models, respectively. Inset: the corresponding first derivatives of ΔE_0^{1h}. (b) Intensity of the spin-polarized single-particle spectral function $|\mathbf{I}_{\max}(\mathbf{k})|$ at $\mathbf{k} = (\pi/2, \pi/2)$ as a function of λ. Here ED results are obtained in a 4×4 lattice under PBC.

model as illustrated in Fig. 10(b). Here the intensity $|\mathbf{I}_{\max}(\mathbf{k})|$ of the spin-polarized spectral function [defined in Eq. (E8) in Appendix E] is shown in Fig. 10(b) at $\mathbf{k} = (\pi/2, \pi/2)$.

APPENDIX D: VARIATIONAL MONTE CARLO PROCEDURE

1. Variational ground state at half-filling

At half-filling, both t-J and $\sigma \cdot t$-J models are reduced to a pure spin-$\frac{1}{2}$ Heisenberg system. At present, the best variational ground state is the so-called Liang-Doucot-Anderson bosonic "resonating valence bond" (RVB) state [24] as

$$|\phi_0\rangle = \sum_v \omega_v |v\rangle, \tag{D1}$$

where each pair of spins in a dimer covering configuration $|v\rangle$ from different sublattices

$$|v\rangle = \sum_{\{\sigma\}} \left(\prod_{(i,j)\in v} \epsilon_{\sigma_i\sigma_j} \right) c^\dagger_{1\sigma_1} \dots c^\dagger_{N\sigma_N} |0\rangle \tag{D2}$$

forms a singlet pairing forced by a Levi-Civita symbol $\epsilon_{\sigma_i\sigma_j}$ or, equivalently, the Marshall sign [29]. During the calculations, the non-negative amplitude ω_v can be factorized as $\omega_v = \prod_{(ij)\in v} h_{ij}$, where h_{ij} is a non-negative function depending on sites i and j. To obtain a ground state for AF spin Heisenberg model, we have to optimize all factors h_{ij}. Conversely, with predetermined h_{ij}, one can artificially tune the background spin correlations ξ. For example, in Fig. 7, we choose a form of h_{ij},

$$h_{ij} = r_{ij}^{-\alpha}, \tag{D3}$$

where r_{ij} being the Manhattan distance $|x_i - x_j| + |y_i - y_j|$ with (x_i, y_i) being a coordinate of site i. The spin correlation length ξ gradually decreases as the parameter α in Eq. (D3) increases. For example, a state with $\alpha = 2$ shows an AF long-range order $\xi \gg L$, as shown in Fig. 1, while a short-range-ordered state with $\xi \sim 2.7$ can be obtained by setting $\alpha = 4$.

2. Variational wave functions for the *t*-*J*-R model

Based on the ground states in Eqs. (B1) and (B2), the wave function $\varphi_{1,2,3,4}(i)$ can be determined by VMC. For example, $\varphi_{1,2}(i)$ will be obtained by diagonalizing the following effective Hamiltonian H_{eff} as the wave function for the composite quasiparticle $\tilde{c}_{i\downarrow}$ defined in Eq. (6):

$$H_{\text{eff}} = -\sum_{\langle i,j \rangle} \tilde{t}_{ij}^{\downarrow} h_i^{\dagger} h_j + \text{H.c.}, \qquad (D4)$$

where $\tilde{t}_{ij}^{\downarrow}$ represents an effective hopping integral

$$\tilde{t}_{ij}^{\downarrow} = t \sum_{\sigma} \langle \phi_0 | \tilde{c}_{j\downarrow}^{\dagger} c_{j\sigma} c_{i\sigma}^{\dagger} \tilde{c}_{i\downarrow} | \phi_0 \rangle. \qquad (D5)$$

Here $\tilde{t}_{ij}^{\downarrow}$ generally takes a complex value due to the phase-shift factor of a twisted particle $\tilde{c}_{i\downarrow} \equiv e^{\mp i\hat{\Omega}_i} c_{i\downarrow}$. Thus, it is a Harper-Hofstadter–type Hamiltonian with a nonuniform flux in Eq. (D4) that breaks the translational symmetry for $\varphi_{1,2}(i)$. Such an emergent flux can induce exotic consequences beyond the simple tight-binding model. In such an effective Hamiltonian, $h_i^{\dagger}$ creates a "twisted" hole with the wave function $\varphi_{1,2}(i)$. Two sectors are available, denoted as $|\Psi\rangle_{1,2}$, respectively, in Eq. (B1), which correctly reproduce two ground states $|\Psi_{\text{G}}\rangle_{1,2}$ with the angular momentum $L_z = \pm 1$. For $S_z = -\frac{1}{2}$, similar constructions $|\Psi\rangle_{3,4}$ in Eq. (B2) lead to two ground states $|\Psi_{\text{G}}\rangle_{3,4}$ with orbital momentum $L_z = \mp 1$. Indeed, excited states can also be determined by Eq. (D4) as one may choose excited wave functions $\varphi_{1,2,3,4}$ determined by Eq. (D5) or artificially tune the spin correlation in $|\phi_0\rangle$ (cf. Appendix D 1).

Now, let us turn on the SOC with $\lambda \neq 0$. As noted above, $L_z = \pm 1$ and $S^z = \pm \frac{1}{2}$ are no longer the good quantum numbers, but the total angular momentum $J_z = L_z + S_z$ remains. Then, one may reconstruct the one-hole ansatz states in terms of the linear combinations between $|\Psi_{\text{G}}\rangle_{1,2,3,4}$ and their excited states. From the symmetry discussed above, Rashba interaction will lift the degeneracy between $|\Psi_{\text{G}}\rangle_{1,3}$ and $|\Psi_{\text{G}}\rangle_{2,4}$ with different J_z's. A ground-state ansatz for the *t*-*J*-R model should come from a linear combination, i.e.,

$$|\Psi_{\text{R}}\rangle_{\text{umdm}} = |\Psi\rangle_1 + |\Psi\rangle_3$$
$$= \sum_i [\varphi_{\downarrow}(i) e^{-i\hat{\Omega}_i} c_{i\downarrow} + \varphi_{\uparrow}(i) e^{-i\hat{\Omega}_i} c_{i\uparrow}] |\phi_0\rangle, \quad (D6)$$

or between $|\Psi\rangle_2$ and $|\Psi\rangle_4$,

$$|\Psi_{\text{R}}\rangle_{\text{updp}} = |\Psi\rangle_2 + |\Psi\rangle_4$$
$$= \sum_i [\varphi_{\downarrow}(i) e^{+i\hat{\Omega}_i} c_{i\downarrow} + \varphi_{\uparrow}(i) e^{+i\hat{\Omega}_i} c_{i\uparrow}] |\phi_0\rangle, \quad (D7)$$

where hole wave functions $\varphi_{\uparrow}$ and $\varphi_{\downarrow}$ are variational parameters and the subscripts "umdm" or "updp" represent chirality of the built-in phase-string factor $e^{\pm i\hat{\Omega}_i}$ with "m" for "−" and "p" for "+" in the front of the removed ↑ spin ("u") or ↓ spin ("d"). The true ground states are variationally proved to be $|\Psi_{\text{R}}\rangle_{\text{umdm}}$ or Eq. (11), and its twofold degeneracy is protected by a time-reversal symmetry $\mathcal{T}$ in Eq. (B3).

Parallel to the ansatz in Eqs. (D6) and (D7), another two recombinations $|\Psi_{\text{R}}\rangle_{\text{umdp}}$ and $|\Psi_{\text{R}}\rangle_{\text{updm}}$ will generate excited states. Therefore, we have four sectors of variational wave functions $|\Psi_{\text{R}}\rangle_{\text{umdm}}$, $|\Psi_{\text{R}}\rangle_{\text{updp}}$, $|\Psi_{\text{R}}\rangle_{\text{updm}}$, and $|\Psi_{\text{R}}\rangle_{\text{umdp}}$. Figure 3(b) shows energies of ground states with $J_z = \pm\frac{3}{2}$ and the first excited states with $J_z = \pm\frac{1}{2}$ over the SOC strength λ via VMC as compared with Fig. 3(a) via ED.

Small Rashba interaction allows perturbative analysis on ground-state wave functions. Conservation of J_z requires the ground states for the *t*-*J*-R model to be composed of one of ground states and one excited state with $L_z = \pm 2$ for the *t*-*J* model. A sufficiently small SOC strength λ will select one chiral spin pattern with total momentum $J_z = \frac{3}{2}$ or $-\frac{3}{2}$, such that $|\Psi_{\text{R}}\rangle_{\text{updp}}$ produces ground states. If we choose $|\Psi\rangle_2$ to be $|\Psi_{\text{G}}\rangle_2$ with $J_z = \frac{3}{2}$, then $|\Psi\rangle_4$ must have a quantum number $L_z = 2$ with $J_z = 2 - \frac{1}{2} = \frac{3}{2}$, which is the first excited state of the *t*-*J* model. If we start with $|\Psi_{\text{G}}\rangle_4$ as a choice for $|\Psi\rangle_4$, then $|\Psi\rangle_2$ is the first excited state of *t*-*J* model with $L_z = -2$. The two ground states can be transformed to each other by time-reversal symmetry $\mathcal{T}$ in Eq. (B3). Technically, as proved by previous ED results [8], nondegeneracy between $|\Psi_{\text{G}}\rangle_{1,2,3,4}$ and first excited states accidentally originates from the open boundary condition, which leads to dramatically large energy gain induced by SOC as compared to the $\sigma \cdot t$-*J*-R model in Figs. 3(a) and 3(b).

APPENDIX E: SPIN-POLARIZED SPECTRAL FUNCTION

The spin-polarized angle-resolved photoemission spectroscopy (ARPES) can be used to detect the spin texture of a quasiparticle (hole) excitation. The normal spectral function for a single quasihole of spin σ is defined by

$$\mathcal{A}_{\sigma}(\omega, \mathbf{k}) = \sum_n \langle \Psi_{\text{G}} | c_{\mathbf{k}\sigma}^{\dagger} | n \rangle \langle n | c_{\mathbf{k}\sigma} | \Psi_{\text{G}} \rangle \delta(\omega - E_n + E_{\text{G}})$$
$$= \frac{1}{\pi} \text{Im} \sum_n \frac{\langle \Psi_{\text{G}} | c_{\mathbf{k}\sigma}^{\dagger} | n \rangle \langle n | c_{\mathbf{k}\sigma} | \Psi_{\text{G}} \rangle}{\omega - E_n + E_{\text{G}} - i\eta}, \qquad (E1)$$

where $|\Psi_{\text{G}}\rangle$ is the ground state with energy E_{G} and $|n\rangle$ denotes an eigenstate of energy E_n with an extra hole created by $c_{\mathbf{k},\sigma}$ on $|\Psi_{\text{G}}\rangle$. In Eq. (E1), η is a broadening introduced to represent energy resolution. Based on $\mathcal{A}_{\sigma}(\omega, \mathbf{k})$, we may further extract information on spin polarization, for example, by focusing on the intensity of the scattered electrons that are parallel or perpendicular to the momentum $\mathbf{k}$. One may define

$$c_{\mathbf{k},\sigma_{\perp}}^{\dagger} = \frac{1}{\sqrt{2}} (c_{\mathbf{k}\uparrow}^{\dagger} + i e^{i\theta_{\mathbf{k}}} c_{\mathbf{k}\downarrow}^{\dagger}), \qquad (E2)$$

$$c_{\mathbf{k},\bar{\sigma}_{\perp}}^{\dagger} = \frac{1}{\sqrt{2}} (c_{\mathbf{k}\uparrow}^{\dagger} - i e^{i\theta_{\mathbf{k}}} c_{\mathbf{k}\downarrow}^{\dagger}) \qquad (E3)$$

to create holes, respectively, with spin polarization at $\mathbf{S}_{\sigma_{\perp}} = (\cos\theta_{\mathbf{k}}, \sin\theta_{\mathbf{k}}, 0)$ and $\mathbf{S}_{\bar{\sigma}_{\perp}} = -\mathbf{S}_{\sigma_{\perp}}$ perpendicular to momentum $\mathbf{k}$ lying in the *x*-*y* plane with $e^{i\theta_{\mathbf{k}}} = \frac{k_x + i k_y}{|\mathbf{k}|}$. Similarly, the two operators

$$c_{\mathbf{k},\sigma_{\parallel}}^{\dagger} = \frac{1}{\sqrt{2}} (c_{\mathbf{k}\uparrow}^{\dagger} + e^{i\theta_{\mathbf{k}}} c_{\mathbf{k}\downarrow}^{\dagger}), \qquad (E4)$$

$$c_{\mathbf{k},\bar{\sigma}_{\parallel}}^{\dagger} = \frac{1}{\sqrt{2}} (c_{\mathbf{k}\uparrow}^{\dagger} - e^{i\theta_{\mathbf{k}}} c_{\mathbf{k}\downarrow}^{\dagger}) \qquad (E5)$$

create holes with spin polarization along $\mathbf{S}_{\sigma_{\parallel}} = (\sin\theta_{\mathbf{k}}, -\cos\theta_{\mathbf{k}}, 0)$ and $\mathbf{S}_{\bar{\sigma}_{\parallel}} = -\mathbf{S}_{\sigma_{\parallel}}$, parallel to

momentum $\mathbf{k}$. Then, the spin polarization $I_{\perp}(\omega, \mathbf{k})$ at the direction perpendicular to momentum $\mathbf{k}$ takes the form

$$I_{\perp}(\omega, \mathbf{k}) = \mathcal{A}_{\sigma_{\perp}}(\omega, \mathbf{k}) - \mathcal{A}_{\bar{\sigma}_{\perp}}(\omega, \mathbf{k}), \qquad \text{(E6)}$$

and $I_{\parallel}(\omega, \mathbf{k})$ at direction parallel to momentum $\mathbf{k}$:

$$I_{\parallel}(\omega, \mathbf{k}) = \mathcal{A}_{\sigma_{\parallel}}(\omega, \mathbf{k}) - \mathcal{A}_{\bar{\sigma}_{\parallel}}(\omega, \mathbf{k}). \qquad \text{(E7)}$$

Finally, one may define an intensity vector $\mathbf{I}_{\max}(\mathbf{k})$

$$\mathbf{I}_{\max}(\mathbf{k}) = I_{\parallel}(\omega_c, \mathbf{k})\mathbf{e}_{\mathbf{k}, \parallel} + I_{\perp}(\omega_c, \mathbf{k})\mathbf{e}_{\mathbf{k}, \perp}, \qquad \text{(E8)}$$

where $\mathbf{e}_{\mathbf{k}, \parallel}$ ($\mathbf{e}_{\mathbf{k}, \perp}$) is the unit vector parallel (perpendicular) to momentum $\mathbf{k}$ and ω_c denotes the frequency at which $\sqrt{I_{\perp}(\omega, \mathbf{k})^2 + I_{\parallel}(\omega, \mathbf{k})^2}$ reaches its maximum value $|\mathbf{I}_{\max}(\mathbf{k})|$. The quantity $\mathbf{I}_{\max}(\mathbf{k})$ as probed by the spin-polarized ARPES experiment can effectively characterize the spin-texture structure in the momentum space, away from the Fermi energy and deep inside the Brillouin zone.

APPENDIX F: FRAGILITY OF SPIN TEXTURE IN A FERMI LIQUID

In a Fermi liquid, the spin texture induced by Rashba SOC is fragile at momentum away from the Fermi surface. In this Appendix, we give a brief discussion.

The Landau's Fermi-liquid theory asserts one-to-one correspondence between a free Fermi gas system and an interacting one. The interaction as scattering between quasiparticles manifests as a self-energy $\Sigma(\omega, \mathbf{k})$ in the Green's function of electrons c_{σ}:

$$\begin{aligned}
\mathcal{G}_{\sigma}(\omega, \mathbf{k}) &= \frac{1}{G_0^{-1}(\omega, \mathbf{k}) - \Sigma(\omega, \mathbf{k})} \\
&= \frac{1}{\omega - [\epsilon_0(\mathbf{k}) - \mu + \text{Re}\Sigma(\omega, \mathbf{k})] - i\Gamma(\omega, \mathbf{k})},
\end{aligned} \qquad \text{(F1)}$$

where $G_0(\omega, \mathbf{k}) = \{\omega - [\epsilon_0(\mathbf{k}) - \mu]\}^{-1}$ denotes the propagator for the noninteracting Hamiltonian H_0, which generally involves both nearest- and next-nearest-neighbor hopping, t

and t' with a dispersion relation $\epsilon_0(\mathbf{k})$,

$$\epsilon_0(\mathbf{k}) = -2t(\cos k_x + \cos k_y) + 4t' \cos k_x \cos k_y. \qquad \text{(F2)}$$

μ is a chemical potential which determines the doping concentration. The imaginary part $\Gamma(\omega, \mathbf{k})$ in Eq. (F1) of the self-energy $\Sigma(\omega, \mathbf{k})$ dominates the lifetime of a quasiparticle excitation. A significant consequence is that to the leading order, $\Gamma(\omega, \mathbf{k})$ depends on the second power of the exciting energy

$$\Gamma(\omega, \mathbf{k}) = c\omega^2, \qquad \text{(F3)}$$

with a coefficient c determined by quasiparticles' scatterings.

A sufficiently weak Rashba SOC interaction, on a reasonable assumption, exerts no influence on the self-energy. In other words, we shall introduce eigenmodes $d_{\mathbf{k}\pm}^{\dagger}$ to diagonalize the free part $H_0 + H_R$,

$$d_{\mathbf{k}\pm}^{\dagger} = \frac{1}{\sqrt{2}}(c_{\mathbf{k}\uparrow}^{\dagger} \pm e^{i\varphi_{\mathbf{k}}}c_{\mathbf{k}\downarrow}^{\dagger}), \qquad \text{(F4)}$$

which, consequently, modify the Green's functions

$$\mathcal{G}_+(\omega, \mathbf{k}) = \frac{1}{G_0^{-1}(\omega, \mathbf{k}) - \Delta_{\mathbf{k}} - i\Gamma(\omega, \mathbf{k})}, \qquad \text{(F5)}$$

$$\mathcal{G}_-(\omega, \mathbf{k}) = \frac{1}{G_0^{-1}(\omega, \mathbf{k}) + \Delta_{\mathbf{k}} - i\Gamma(\omega, \mathbf{k})}. \qquad \text{(F6)}$$

Here, $\Delta_{\mathbf{k}} = 2\lambda\sqrt{\sin^2 k_x + \sin^2 k_y}$ is the energy splitting induced by SOC in H_R, and $e^{i\varphi_{\mathbf{k}}} = \frac{\sin k_x + i \sin k_y}{\sqrt{\sin^2 k_x + \sin^2 k_y}}$.

Follow the procedure presented in Appendix E and we can obtain the spin polarization perpendicular to the momentum $\mathbf{k}$:

$$\begin{aligned}
I_{\perp}(\omega_c, \mathbf{k}) &= \mathcal{A}_{\sigma_{\perp}}(\omega_c, \mathbf{k}) - \mathcal{A}_{\bar{\sigma}_{\perp}}(\omega_c, \mathbf{k}) \\
&= 2\cos(\theta_{\mathbf{k}} - \varphi_{\mathbf{k}})\frac{2\Delta_{\mathbf{k}}}{c\epsilon_{\mathbf{k}}^2(c\epsilon_{\mathbf{k}}^2 + \Delta_{\mathbf{k}})}, \qquad \text{(F7)}
\end{aligned}$$

where ω_c is defined in Eq. (E8) to relate to the maximal spectral function $\mathbf{I}_{\max}(\mathbf{k})$ and $e^{i\theta_{\mathbf{k}}} = \frac{k_x + ik_y}{|\mathbf{k}|}$. Since $\Delta_{\mathbf{k}}$ is very small, a quasiparticle with momentum away from Fermi surface towards Γ point makes a vanishing contribution, which is depicted in Fig. 8 with parameters $c = 0.005$, $\lambda = 0.01J$, and $t' = 0.2t$.

[1] P. W. Anderson, The resonating valence bond state in La$_2$CuO$_4$ and superconductivity, Science **235**, 1196 (1987).

[2] P. A. Lee, N. Nagaosa, and X.-G. Wen, Doping a Mott insulator: Physics of high-temperature superconductivity, Rev. Mod. Phys. **78**, 17 (2006).

[3] B. I. Shraiman and E. D. Siggia, Mobile Vacancies in a Quantum Heisenberg Antiferromagnet, Phys. Rev. Lett. **61**, 467 (1988).

[4] S. Schmitt-Rink, C. M. Varma, and A. E. Ruckenstein, Spectral Function of Holes in a Quantum Antiferromagnet, Phys. Rev. Lett. **60**, 2793 (1988).

[5] C. L. Kane, P. A. Lee, and N. Read, Motion of a single hole in a quantum antiferromagnet, Phys. Rev. B **39**, 6880 (1989).

[6] G. Martinez and P. Horsch, Spin polarons in the t-J model, Phys. Rev. B **44**, 317 (1991).

[7] Z. Liu and E. Manousakis, Spectral function of a hole in the t-J model, Phys. Rev. B **44**, 2414 (1991).

[8] W. Zheng, Z. Zhu, D. N. Sheng, and Z.-Y. Weng, Hidden spin current in doped Mott antiferromagnets, Phys. Rev. B **98**, 165102 (2018).

[9] Z. Zhu, D. N. Sheng, and Z.-Y. Weng, Intrinsic translational symmetry breaking in a doped Mott insulator, Phys. Rev. B **98**, 035129 (2018).

[10] Z. Zhu and Z.-Y. Weng, Quasiparticle collapsing in an anisotropic t-J ladder, Phys. Rev. B **92**, 235156 (2015).

[11] Q.-R. Wang, Z. Zhu, Y. Qi, and Z.-Y. Weng, Variational wave function for an anisotropic single-hole-doped t-J ladder, arXiv:1509.01260.

[12] S. Chen, Q.-R. Wang, Y. Qi, D. N. Sheng, and Z.-Y. Weng, Single-hole wave function in two dimensions: A case study of the doped Mott insulator, Phys. Rev. B **99**, 205128 (2019).

[13] K. Gotlieb, C.-Y. Lin, M. Serbyn, W. Zhang, C. L. Smallwood, C. Jozwiak, H. Eisaki, Z. Hussain, A. Vishwanath, and A. Lanzara, Revealing hidden spin-momentum locking in a high-temperature cuprate superconductor, Science **362**, 1271 (2018).

[14] J.-H. Zhang, S. Li, Y. Ma, Y. Zhong, H. Ding, and Z.-Y. Weng, Phenomenological single-particle Green's function for the pseudogap and superconducting phases of high-T_c cuprates, Phys. Rev. Research **2**, 023398 (2020).

[15] F. C. Zhang and T. M. Rice, Effective Hamiltonian for the superconducting Cu oxides, Phys. Rev. B **37**, 3759 (1988).

[16] D. N. Sheng, Y. C. Chen, and Z. Y. Weng, Phase String Effect in a Doped Antiferromagnet, Phys. Rev. Lett. **77**, 5102 (1996).

[17] Z. Y. Weng, D. N. Sheng, Y.-C. Chen, and C. S. Ting, Phase string effect in the t-J model: General theory, Phys. Rev. B **55**, 3894 (1997).

[18] K. Wu, Z. Y. Weng, and J. Zaanen, Sign structure of the t−J model, Phys. Rev. B **77**, 155102 (2008).

[19] Z. Zhu, H.-C. Jiang, Y. Qi, C. Tian, and Z.-Y. Weng, Strong correlation induced charge localization in antiferromagnets, Sci. Rep. **3**, 2586 (2013).

[20] Z. Zhu, H.-C. Jiang, D. N. Sheng, and Z.-Y. Weng, Nature of strong hole pairing in doped Mott antiferromagnets, Sci. Rep. **4**, 5419 (2014).

[21] E. I. Rashba, Theory of electrical spin injection: Tunnel contacts as a solution of the conductivity mismatch problem, Phys. Rev. B **62**, R16267 (2000).

[22] Z.-Y. Weng, Mott physics, sign structure, ground state wavefunction, and high-T_c superconductivity, Front. Phys. **6**, 370 (2011).

[23] Z.-Y. Weng, Superconducting ground state of a doped Mott insulator, New J. Phys. **13**, 103039 (2011).

[24] S. Liang, B. Doucot, and P. W. Anderson, Some New Variational Resonating-Valence-Bond-Type Wave Functions for the Spin-½ Antiferromagnetic Heisenberg Model on a Square Lattice, Phys. Rev. Lett. **61**, 365 (1988).

[25] L. Zhang and Z.-Y. Weng, Sign structure, electron fractionalization, and emergent gauge description of the Hubbard model, Phys. Rev. B **90**, 165120 (2014).

[26] S. Chen, Z. Zhu, and Z.-Y. Weng, Two-hole ground state wavefunction: Non-BCS pairing in a t−J two-leg ladder, Phys. Rev. B **98**, 245138 (2018).

[27] J.-Y. Zhao, S. A. Chen, H.-K. Zhang, and Z.-Y. Weng, Two-hole ground state: Dichotomy in pairing symmetry, arXiv:2106.14898.

[28] A. Bohrdt, E. Demler, and F. Grusdt, Rotational Resonances and Regge-Like Trajectories in Lightly Doped Antiferromagnets, Phys. Rev. Lett. **127**, 197004 (2021).

[29] A. Auerbach, *Interacting Electrons and Quantum Magnetism* (Springer, Berlin, 1994).